Numerical CFD Comparison of Lillgrund Employing RANS

Simisiroglou, N.; Breton, S.-P.; Crasto, G.; Hansen, Kurt Schaldemose; Ivanell, S.

Published in:
Energy Procedia

Link to article, DOI:
10.1016/j.egypro.2014.07.242

Publication date:
2014

Document Version
Publisher's PDF, also known as Version of record

Available online at www.sciencedirect.com

ScienceDirect

Energy Procedia 53 (2014) 342 – 351

Energy Procedia

EERA DeepWind'2014, 11th Deep Sea Offshore Wind R&D Conference

Numerical CFD comparison of Lillgrund employing RANS

N. Simisiroglou[a,b], S.-P. Breton[b], G. Crasto[a], K.S. Hansen[c], S. Ivanell[b]

[a]*WindSim AS, Fjordgaten 15, Tønsberg N-3125, Norway*
[b]*Uppsala University Campus Gotland, Visby SE 621 67, Sweden*
[c]*Technical University of Denmark, Nils Koppels Alle 403, Kgs. Lyngby DK 2800 , Denmark*

Abstract

The following article will validate the results obtained using the actuator disc method in the state of the art numerical Computational Fluid Dynamic (CFD) tool WindSim using on-site measurements from the offshore wind farm Lillgrund. WindSim solves the mass, momentum and energy conservation equations using the Reynolds Average Navier Stokes (RANS) method. Emphasis will be put here on investigating how the choice of different parameters influences the results, and comparisons will be performed with experimental data. The quantity that will be compared is the individual energy production of the wind turbines for different grid resolutions, inflow angles, thrust radial distributions and turbulence closure models.

Selection and peer-review under responsibility of SINTEF Energi AS

Keywords: CFD; WindSim; RANS; Actuator Disc; Wakes; Turbulence; Lillgrund

Nomenclature

D	Turbine rotor diameter
$u_{i,\infty}$	Free stream velocity at the porous cell
α_i	Axial induction factor assigned to the porous cell
$u_{I,i}$	Wind velocity at the porous cell of the disc
$C_{T,i}$	Thrust coefficient defined at the porous cell
t_i	Individual thrust of the porous cell
T	Total thrust of the disc
ρ	Air density
σ	Standard deviation
σ_{rel}	Normalized standard deviation
P_f	Power output of the wind turbine located at the front of the row based on experimental data

* Corresponding author. Tel.: +46 72 903 8821.
E-mail address:nikolaos.simisiroglou@windsim.com

Selection and peer-review under responsibility of SINTEF Energi AS
doi:10.1016/j.egypro.2014.07.242

1. Introduction

The tendency towards ever growing offshore wind farms introduces the necessity of accurate wind flow modeling of wind turbine wakes for layout optimization purposes. As the computational power of modern CPUs increases, previously impractical numerical CFD models are gaining more and more ground in the industry, enabling developers to accurately capture the wind flow and wake interaction within the farm. This insight in the wake flow is further utilized to optimize wind farm layouts for higher energy production and lower fatigue loads on wind turbines, making wind farms more economically competitive. Thus, there has been great interest in researching CFD modeling for wind farms [1–3] in recent years.

The Lillgrund offshore wind farm in Öresund is considered a special case as its wind turbines are placed in close proximity to each other, between 3.3 to 4.3 rotor diameters. This layout produces noteworthy wake interactions between wind turbines, making Lillgrund a highly interesting wind farm to study. Recent work investigating the wake interactions for Lillgrund has been performed using Large Eddy Simulations with the research code EllipSys3D developed at DTU [4]. The results showed a high accuracy compared to experimental data, however the major drawback of this code is the high computational resources needed to perform the simulations.

WindSim is a commercial wind farm development tool that solves the mass, momentum and energy conservation equations by the Reynolds Average Navier Stokes (RANS) method. The finite volume method is employed to discretize the RANS equations, and the flow is assumed incompressible. The presence of the wind turbine rotors in the simulations is modeled using the actuator disc method, which models the swept area of the wind turbine as a porous disc. Each porous cell of the disc acts as a momentum sink extracting energy from the flow. The thrust on the disc may be distributed with a uniform, parabolic or polynomial distribution and is calculated from the thrust coefficient curve of the turbine provided by the manufacturer. Studies using this method for wake modeling have been performed using a number of arrangements, such as a single wake [5] or for a group of turbines [6].

The aim of this research is to compare the power production of each wind turbine calculated using the actuator disc method against experimental data for a large offshore wind farm consisting of 48 wind turbines placed in close proximity in order to validate the computational method. In this study, a grid sensitivity study will be performed, and different parameters will be evaluated for their influence in the final power estimation. The parameters that will be evaluated are two different thrust radial distributions, four different turbulence closure models and 21 different inflow directions.

2. Numerical model

In the simulations WindSim 6.0 is used where the RANS equations are solved by the coupled solver MIGAL [7]. WindSim uses PHOENICS, a general purpose CFD solver, to solve the RANS equations in an iterative way. The flow variables that are solved are namely the pressure, the three velocity components, the turbulent kinetic energy and the turbulent dissipation rate. Different turbulent closures are available in WindSim; in this report the k-epsilon with YAP correction[8], the RNG k-epsilon[9], the standard k-epsilon and the modified k-epsilon [10] will be used and compared.

The actuator disc thrust is calculated from the wind speed at the i-th porous cell of the disc at each iteration in the following way. A lookup table connecting the velocity at a given cell of the actuator disc $u_{1,i}$, and the corresponding thrust coefficient defined at this cell, $C_{T,i}$, is created. This is done by usage of the one dimensional momentum theory and the thrust coefficient curve provided by the turbine manufacturer. Note that the thrust coefficient curve provided by the manufacturer is given as a function of the free stream velocity. Then for each $C_{T,i}$, at a specific freestream velocity $u_{\infty,i}$,an axial induction factor α_i is assigned through equation (2.1). This in turn through equation (2.2) corresponds to a specific wind velocity $u_{1,i}$ at the i-th porous cell of the disc. Thus, a connection between the wind speed of the i-th porous cell at the disc and the thrust coefficient is created.

$$a_i = \frac{1}{2}\left(1-\sqrt{1-C_{T,i}}\right) \quad (2.1)$$

$$u_{\infty,i} = \frac{1}{1-a_i}u_{1,i} \Leftrightarrow u_{1,i} = (1-a_i)u_{\infty,i} \quad (2.2)$$

The lookup table obtained this way is used to interpolate the value of $C_{T,i}$ corresponding to the value of $u_{1,i}$ at the i-th porous cell of the disc, which in turn is used to calculate the thrust t_i acting on this cell from equation 2.3.

$$t_i = C_{T,i}\frac{1}{2}\rho u_{\infty,i}^2 A_i \Rightarrow t_i = C_{T,i}(u_{1,i})\frac{1}{2}\rho\left(\frac{1}{1-a_i(u_{1,i})}u_{1,i}\right)^2 A_i \quad (2.3)$$

Where A_i is the area of the porous cell.

The total axial thrust T on the rotor disc is then calculated from equation (2.4).

$$T \approx \sum_i t_i \quad (2.4)$$

The axial thrust may then be distributed using three different ways in WindSim; the uniform distribution, the parabolic distribution with a maximum value at the hub and zero at the tip and the 4th order polynomial distribution with a zero value at the tip, a maximum value at the mid span and a value that is half of the maximum at the hub position.

2.1. Setup of the simulations

The 2.3 MW Siemens SWT-2.3-93 wind turbines are placed according to the Vattenfall Vindkraft AB online report [11] in eight rows (A to H) with a characteristic gap for row D and E at the area where wind turbine D-05 and E-05 should have been placed, see Figure 1.

Fig. 1 Location of the 48 wind turbines in Lillgrund, inflow sector 120 ± 2.5 degrees. [10]

The domain used for the simulation has dimensions of 4.5 km x 4.5 km. A refinement of the grid is defined for the domain containing the actuator discs, while outside this equidistant region the resolution expands. The equidistant region is automatically defined by the software after the wind turbine locations are selected. In this study a grid resolution of $D/6$ and $D/8$ is achieved in the equidistant region in both the vertical and horizontal directions, with D the diameter of the rotor. A total of 135 cases were produced and analyzed. The parameters investigated are two different radial thrust distributions, i.e. uniform and polynomial, for each different turbulence closure method and for three main direction that are 120 degrees, 222 degrees and 300 degrees. Around each main direction, two sets of three additional angles separated by 5 degrees intervals are further simulated. For example the 120 degrees inflow angle is further simulated for angles of 105^0, 110^0, 115^0, 125^0, 130^0, 135^0. The input conditions used in the simulation were chosen to match the available experimental data and are presented in Table 1.

Table 1 Input conditions used in the simulations

Inflow direction	Wind Speed (m/s)	TI (%)
Northwest case 300 degrees	9	6.0
Southeast case 120 degrees	9	7.8
Southwest case 222 degrees	9	5.6

2.2. Data

The filtering of the measurement data is performed according to recommended practices [12]. The angular width and wind velocity considered for each flow sector are respectively ± 2.5 degrees and 9.0 ± 0.5 m/s. For the flow sector 105-135 degrees the

turbulence intensity is 7.8%, whereas for the flow sector 207-237 degrees it is 5.6%, and 6% for the flow sector 285-315 degrees. A summary of the conditions considered for the flow sector 105-135 degrees is shown in Table 2.

Table 2 Example of the flow cases for directions of 105-135 degrees

Flow Sector	Wind Speed (m/s)	TI (%)
105.0 ±2.5 degrees	9.0 ±0.5 m/s	7.8
115.0 ±2.5 degrees	9.0 ±0.5 m/s	7.8
120.0 ±2.5 degrees	9.0 ±0.5 m/s	7.8
125.0 ±2.5 degrees	9.0 ±0.5 m/s	7.8
130.0 ±2.5 degrees	9.0 ±0.5 m/s	7.8
135.0 ±2.5 degrees	9.0 ±0.5 m/s	7.8

3. Results

The results that will be presented in this section are for row 3 and 5 considering an inflow angle of 120 degrees and for row B, D and E considering an inflow angle of 222 degrees. The error bars related to the experimental data have been calculated using the normalized standard deviation, denoted σ_{rel} according to the following relation:

$$\sigma_{rel} = \frac{\sigma}{P_f} \quad (2.5)$$

Where σ is the standard deviation of the measurements and P_f the average experimental measured power output of the wind turbine located at the front of the row subject to the undisturbed wind flow. For all the figures in the remaining article the error bars are calculated by expression (2.5) and the power output of all wind turbines are normalized by dividing the power output of each wind turbine by P_f .

As may be observed in Figure 2 the power outputs obtained from using a resolution of D/6 and D/8 show significant differences. This outcome indicates that the results are not yet grid independent and a higher resolution should be used. A resolution of D/8 will be assumed for the remainder of the article.

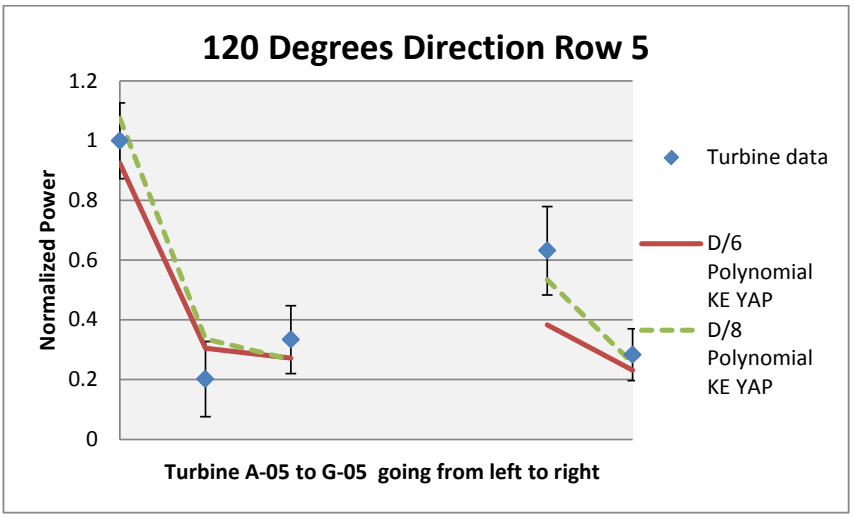

Fig. 2 Power predicted using two different resolutions D/6 and D/8 versus experimental power data retrieved from Lillgrund for 120 ± 2.5 degrees and 9.0 ± 0.5 m/s when using the polynomial distribution and the k-epsilon with YAP corrections turbulence closure model.

The results obtained for different rows and wind flow directions by using different thrust distributions, i.e. a polynomial and a uniform distribution, where the k-epsilon with YAP correction turbulence closure is employed are illustrated in Figure 3 to 7. From these figures it seems that the simulations performed using the polynomial distribution of the thrust over predict the power output of the first wind turbine, especially for the case illustrated in Figure 6, while the results using the uniform distribution seem to be fairly accurate for the first wind turbine in all figures. An exception to this may be seen in Figure 7 where the polynomial distribution does not over predict the power output from the first wind turbine whereas the uniform distribution under predicts it. The power estimation of the second wind turbine in some cases is overestimated as seen in Figure 3 and Figure 4 and in other cases it is underestimated, Figure 5 and Figure 6. Furthermore, the power estimation of the subsequent turbines seems to be under predicted when using either thrust distributions. The polynomial distribution is giving result of higher accuracy in comparison to the uniform one, especially for the cases presented in Figure 4 and Figure 7. Here the wake recovery due to the wind turbine gap is captured with higher precision for simulations using the polynomial distribution in comparison to the uniform distribution. It should be noted that the power increase from the second to the third wind turbine was not captured in any figure. As illustrated in Figure 6 this has caused a noticeable difference between the simulated power output and the experimental power data for the third and fourth wind turbines, D-06 and D-04 respectively. Furthermore, this difference was further increased for the fourth wind turbine as the wake recovery was underestimated.

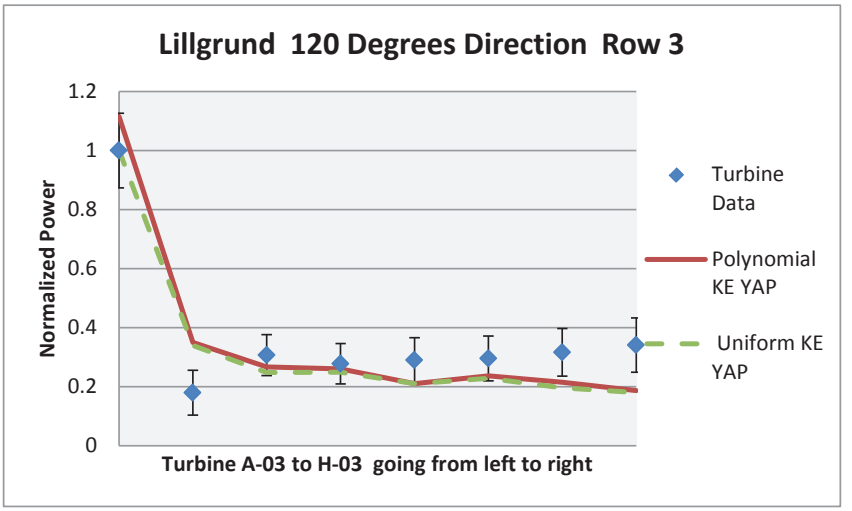

Fig. 3 Power predicted by two different thrust distributions for a resolution of D/8 versus experimental power data retrieved from Lillgrund for 120 ± 2.5 degrees and 9.0 ± 0.5 m/s when using the k-epsilon with YAP correction turbulence closure model.

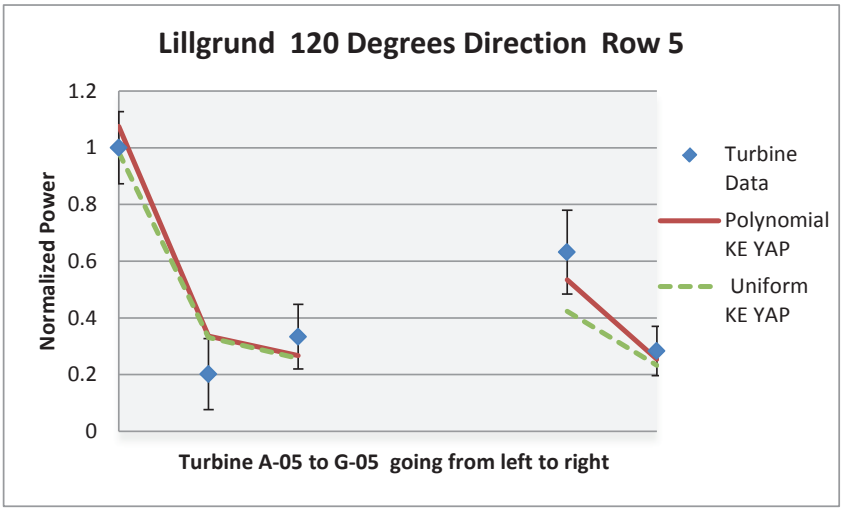

Fig. 4 Power predicted by two different thrust distributions for a resolution of D/8 versus experimental power data retrieved from Lillgrund for 120 ± 2.5 degrees and 9.0 ± 0.5 m/s when using the k-epsilon with YAP correction turbulence closure model.

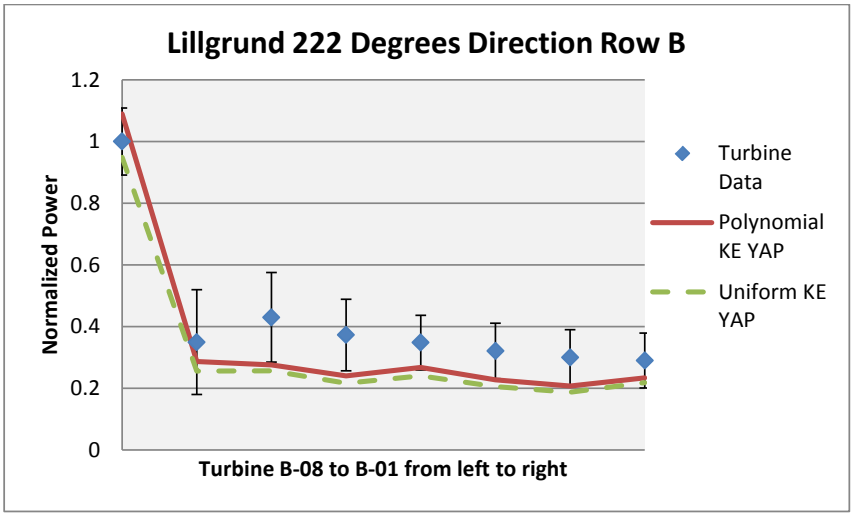

Fig. 5 Power predicted by two different thrust distributions for a resolution of D/8 versus experimental power data retrieved from Lillgrund for 222 ± 2.5 degrees and 9.0 ± 0.5 m/s when using the k-epsilon with YAP correction turbulence closure model.

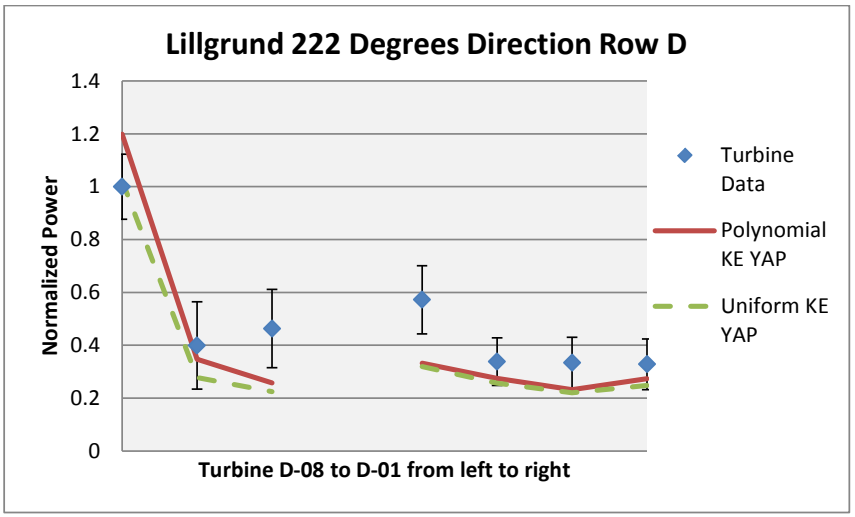

Fig. 6 Power predicted by two different thrust distributions for a resolution of D/8 versus experimental power data retrieved from Lillgrund for 222 ± 2.5 degrees and 9.0 ± 0.5 m/s when using the k-epsilon with YAP correction turbulence closure model.

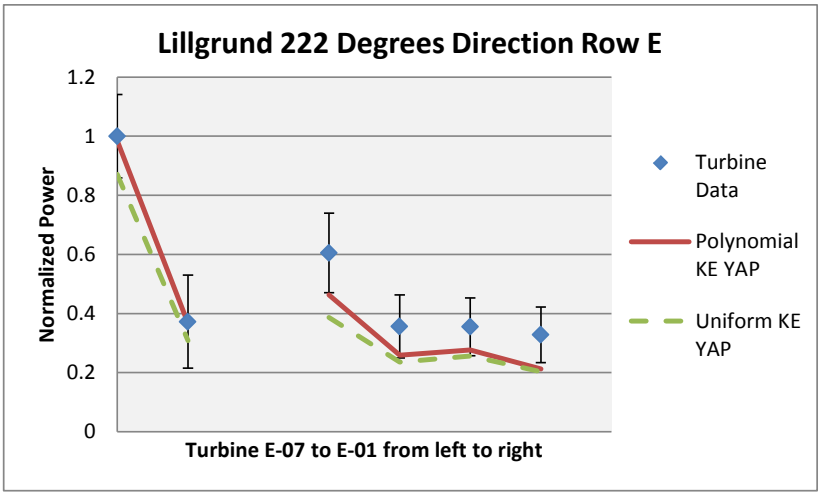

Fig. 7 Power predicted by two different thrust distributions for a resolution of D/8 versus experimental power data retrieved from Lillgrund for 222 ± 2.5 degrees and 9.0 ± 0.5 m/s when using the k-epsilon with YAP correction turbulence closure model.

The influence of different closure models is also investigated. The results obtained with the usage of four different closure models may be seen in Figure 8 to Figure 12 for different rows and wind flow directions. Different turbulent closure models produced different power estimations, with the standard k-epsilon, modified k-epsilon and k-epsilon with YAP correction models in most cases performing similarly or better than the RNG k-epsilon model. Specifically, it can be seen that the power estimation of the first wind turbine in the row is almost identical for all different turbulence models. However, downstream of the first wind turbine the results differ significantly. At the second wind turbine the power deficit is substantially larger when using the RNG k-epsilon model in comparison to the other closure models which perform similarly. The power estimations for the wind turbines following the second wind turbine of the row is in all cases more accurately predicted when using the standard k-epsilon, modified k-epsilon and k-epsilon with YAP correction models, than when using the RNG k-epsilon model. The power prediction difference of the RNG k-epsilon model in comparison with the other turbulence closure models for the subsequent wind turbines may be attributed to the lower power estimation of the second wind turbine in the row. A noteworthy result is presented in Figure 11. Here the power estimation of the first wind turbine, D-08, is 19.4% to 21.3% higher for all different closure models compared to the turbine data. For the second wind turbine, D-07, the RNG k-epsilon model seems to over predict the power deficit, whereas the results from the other closure models are within the error bars. The increase in power output of the third wind turbine, similarly to Figure 6, was not captured, leading to larger discrepancies between simulation and experimental data for the third and fourth wind turbines, D-06 and D-04 respectively. However, even though the power estimations are under predicted for the third and the fourth wind turbines, the increase in the power production due to the wake recovery in the gap is over predicted when using the RNG k-epsilon model, whereas the other turbulence models under predict this power increase.

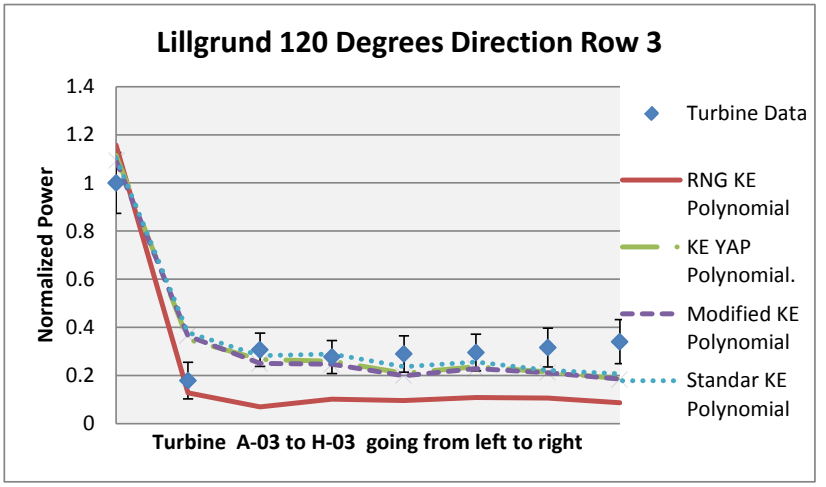

Fig. 8 Power predicted for four different turbulence models for a resolution of D/8 versus experimental power data retrieved from Lillgrund for 120 ± 2.5 degrees and 9.0 ± 0.5 m/s for the polynomial distribution.

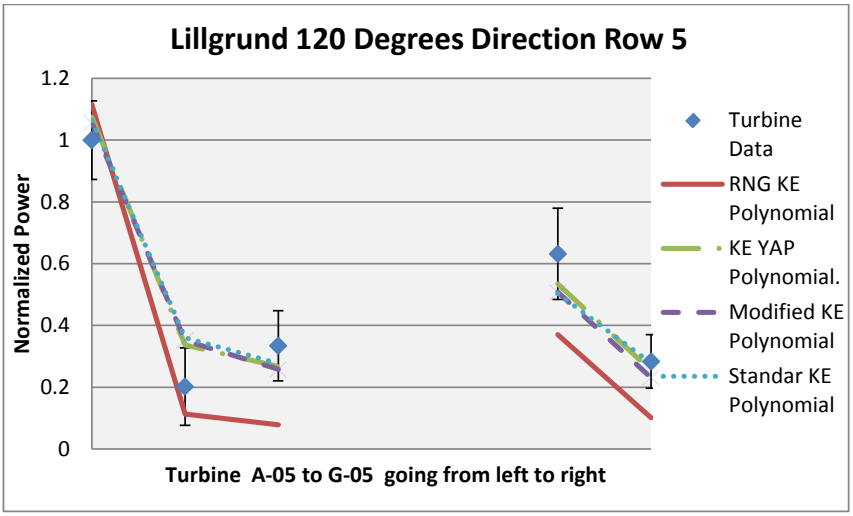

Fig. 9 Power predicted for four different turbulence models for a resolution of D/8 versus experimental power data retrieved from Lillgrund for 120 ± 2.5 degrees and 9.0 ± 0.5 m/s for the polynomial distribution.

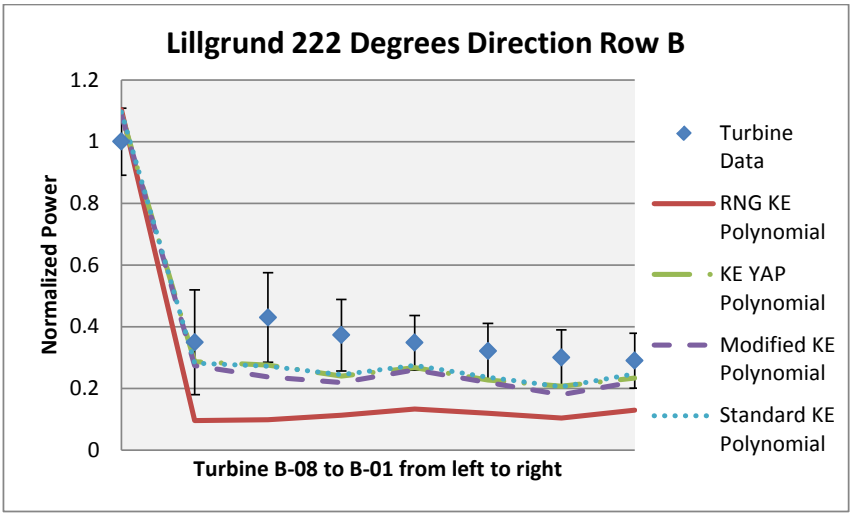

Fig. 10 Power predicted for four different turbulence models for a resolution of D/8 versus experimental power data retrieved from Lillgrund for 222 ± 2.5 degrees and 9.0 ± 0.5 m/s for the polynomial distribution.

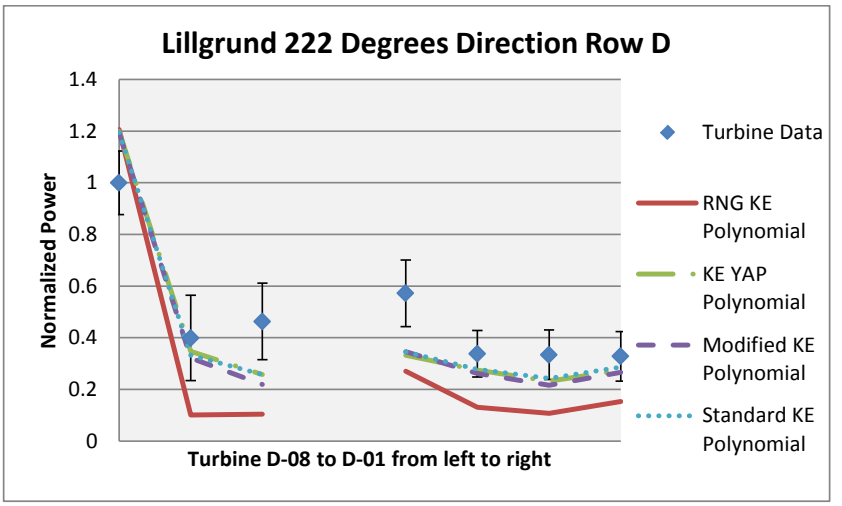

Fig. 11 Power predicted for four different turbulence models for a resolution of D/8 versus experimental power data retrieved from Lillgrund for 222 ± 2.5 degrees and 9.0 ± 0.5 m/s for the polynomial distribution.

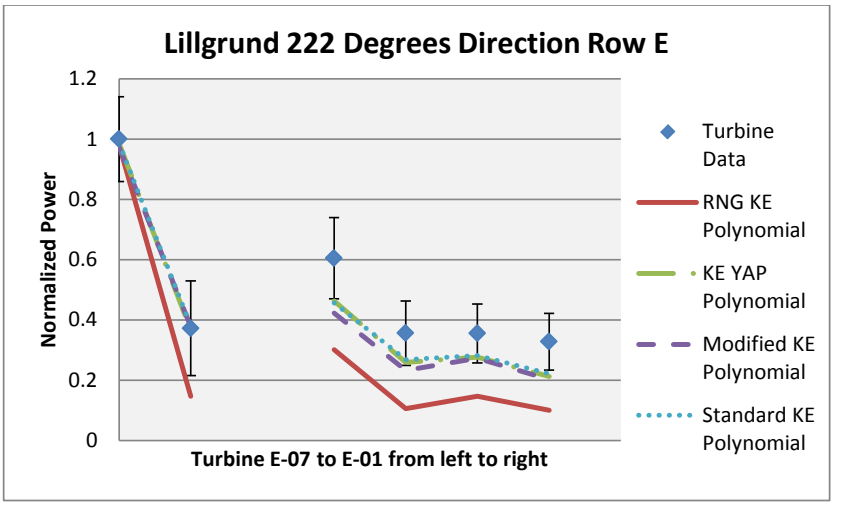

Fig. 12 Power predicted for four different turbulence models for a resolution of D/8 versus experimental power data retrieved from Lillgrund for 222 ± 2.5 degrees and 9.0 ± 0.5 m/s for the polynomial distribution.

4. Discussion and Conclusion

The results presented above were selected considering the high number of experimental observations available and the peculiar phenomena induced by the wind turbine gap; however they are a fraction of the total results simulated. As illustrated in Figure 2, the simulations capture the decrease in power production at the second wind turbine due to the wake of the first turbine, as well as the restored wind flow for wind turbine F-05 due to the missing wind turbines in the gap. Further, the power estimations are within one standard deviation of the experimental data. In almost all cases the results achieved using the higher grid resolution, D/8, outperform those obtained using the lower resolution simulation D/6 indicating firstly the need for high resolution simulations for accurate power predictions and secondly acting as an encouraging indicator that for higher resolutions the physics governing the wake may be captured in a more precise way. The polynomial distribution, by representing more accurately the thrust force distribution on the rotor, seems to lead to results of higher accuracy in comparison to the uniform distribution. The flow recovery in most cases is adequately captured see Figure 9 and Figure 12, although this is not prominently the case for the results presented in Figure 11. Overall it is observed that there is an overestimation of the wake effects especially

when using the RNG k-epsilon model and looking at the first two wind turbines of the row. The overestimation of the wake effects for all turbulence models may partially be enforced from the assumption of a neutrally stratified atmospheric boundary layer in the simulations that is not the general case in reality. Further concerning the different turbulent closure models, it seems that the RNG k-epsilon captures in some cases the power production in the second wind turbine more accurately than the other turbulence models but underestimates the power production for the following wind turbines of the row. The lower power estimation when using the RNG k-epsilon closure model in comparison to other closure models is most likely linked to the lower turbulence kinetic energy produced when using this model. It should be noted that the power increase from the second to the third wind turbine has not been captured in any analysed case up to now by the model. Finally regarding the standard k-epsilon, modified k-epsilon and k-epsilon with YAP correction when using the polynomial distribution of the thrust, it seems that these models tend to overestimate the power output of the first and second wind turbine in the row but capture the power output for the subsequent wind turbines more accurately than the RNG k-epsilon.

Future research will focus on the first three wind turbines in the row; accurate power estimations of the first three wind turbines seem to play a major role in accurately estimating the power production of all subsequent wind turbines in the row itself. Therefore a thorough investigation as to why the polynomial distribution is overestimating the power output of the first wind turbine, why the simulations do not capture the power increase from the second to the third wind turbine and why the power deficit when using the RNG-k epsilon is so high will be performed. Furthermore, additional analysis of the total amount of simulated result in further search for general trends will be executed. Moreover research will be directed on how to include meandering and swirl effects of the wakes in the CFD model used in this analysis. Finally, studies with higher grid resolutions will be performed and comparison with analytical models and LES models will be conducted.

Acknowledgments

The authors acknowledge Vattenfall AB for the permission to use the SCADA data from the Lillgrund offshore wind farm and the Research Council of Norway for their financial support.

References

[1] K. Rados, G. Larsen, R. Barthelmie, W. Schlez, B. Lange, G. Schepers, et al., Comparison of Wake Models with Data for Offshore Windfarms, Wind Eng. 25 (2009) 271–280.

[2] R. Barthelmie, K. Hansen, S. Frandsen, O. Rathmann, J.G. Schepers, W. Schlez, et al., Modelling and measuring flow and wind turbine wakes in large wind farms offshore, Wind Energy. 12 (2009) 431–444.

[3] A. Crespo, J. Hernandez, S. Frandsen, Survey of Modelling Methods for Wind Turbine Wakes and Wind Farms, Wind Energy. 24 (1999) 1–24.

[4] K. Nilsson, S. Ivanell, K.S. Hansen, R. Mikkelsen, J.N. Sørensen, S.-P. Breton, et al., Large-eddy simulations of the Lillgrund wind farm, Wind Energy. (2014).

[5] G. Crasto, A.R. Gravdahl, CFD wake modeling using a porous disc, in: EWEC, Brussels, 2008.

[6] F. Castellani, A.R. Gravdahl, G. Crasto, E. Piccioni, A. Vignaroli, A Practical Approach in the CFD Simulation of Off-shore Wind Farms through the Actuator Disc Technique, Energy Procedia. 35 (2013) 274–284.

[7] M. Ferry, New Features of MIGAL solver, 9th Int. PHOENICS Users Conf., Moscow, 2002.

[8] C.J. Yap, Turbulent Heat and Momentum Transfer in Recirculating and Impinging Flows, PhD Thesis, University of Manchester, 1987.

[9] V. Yakhot, S.A. Orszag, S. Thangam, T.B. Gatski, C.G. Speziale, Development of turbulence models for shear flows by a double expansion technique, Phys. Fluids A Fluid Dyn. 4 (1992) 1510.

[10] A.R. Gravdahl, Meso Scale Modeling with a Reynolds Averaged Navier Stokes Solver Assessment of wind resources along the Norwegian coast, (1998).

[11] J.-Å. Dahlberg, Assessment of the Lillgrund Windfarm Power Performance Wake Effects Lillgrund, 6_1 LG Pilot Report, 2009.

[12] R. Barthelmie, S. Frandsen, O. Rathmann, K. Hansen, E.S. Politis, J. Prospathopoulos, et al., Flow and wakes in large wind farms : Final report for UpWind WP8 Risø-R-Report, 2011.